30th International Cosmic Ray Conference

The UHECR spectrum measured at the Pierre Auger Observatory and its astrophysical implications

T.Yamamoto[1] for the Pierre Auger Collaboration[2]
[1] *KICP, Enrico Fermi Institute, University of Chicago, Chicago IL USA*
[2] *Pierre Auger Observatory, Av San Martín Norte 304,(5613) Malargüe, Argent*
yamamoto@oddjob.uchicago.edu

Abstract: The Southern part of the Pierre Auger Observatory is nearing completion, and has been in stable operation since January 2004 while it has grown in size. The large sample of data collected so far has led to a significant improvement in the measurement of the energy spectrum of UHE cosmic rays over that previously reported by the Pierre Auger Observatory, both in statistics and in systematic uncertainties. We summarize two measurements of the energy spectrum, one based on the high-statistics surface detector data, and the other of the hybrid data, where the precision of the fluorescence measurements is enhanced by additional information from the surface array. The complementarity of the two approaches is emphasized and results are compared. Possible astrophysical implications of our measurements, and in particular the presence of spectral features, are discussed.

UHE cosmic ray energy spectrum

The Pierre Auger Observatory measures extensive air showers induced by the highest energy events ($E > 10^{18}$ eV) using two detection techniques. Firstly, a collection of telescopes is used to measure the ultraviolet fluorescence light produced when electrons in the shower excite nitrogen molecules in the atmosphere. This technique will be referred as FD (Fluorescence Detector). It measures the longitudinal development of the air-shower and can only be used during dark and moonless nights, yielding a duty cycle of roughly 10%. The second technique (called SD for Surface Detector) uses an array of water Cherenkov detectors to sample the shower front at ground level. The SD has a duty cycle of 100% and the detection efficiency is 100% for energies above $10^{18.5}$ eV ($10^{18.8}$ eV) at zenith angles below (above) 60°. The showers recorded by the SD are quantified in size using the reconstructed signal at 1000 m from the shower axis, called S(1000) [4]. At large zenith angles (above 60°), due to deflection of the shower particles in the geomagnetic field, another energy estimator N_{19} is used [2]. The conversion from these two SD estimators to the primary energy could be calculated using full Monte Carlo simulations but the lack of knowledge of the primary mass and the uncertainties in the hadronic models introduce large systematics. Therefore we use a subset of showers called *hybrid* events that are detected by both the SD and the FD. The conversion parameters from the SD estimators to the energy measured by the FD then is derived experimentally. A comparison of the results of this calibration with the expectations from Monte Carlo simulation can be found in [8]. The FD measures fluorescence light in proportion to the energy deposited by the shower, and so the technique is calorimetric. There is, however, a small correction to account for the energy deposited in the ground by high energy muons and neutrinos. This "invisible energy" correction has a small dependence on mass and hadronic model. The applied correction is based on the average for proton and iron showers from the QGSJet model. This correction factor is about 10% and its systematic uncertainty contributes 4% to the total uncertainty in FD energy [16, 10].

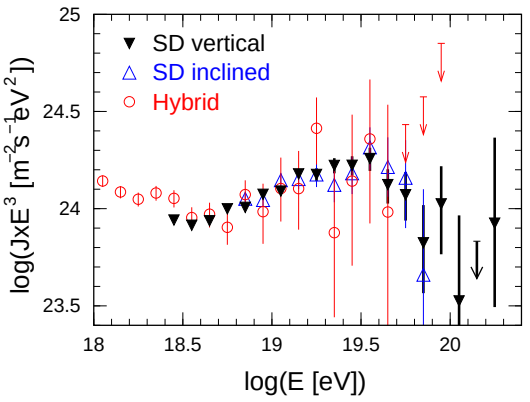

Figure 1: The energy spectrum multiplied by E^3 derived from SD using showers at zenith angles above (filled triangles) and below (opened triangles) 60° ([5, 7]), together with the spectrum derived from the hybrid data set (red circles)[3]. Arrows indicate 84% CL upper-limits.

Fig. 1 shows the energy spectrum multiplied by E^3 from SD data using showers at zenith angles above and below 60° ([5, 7]), together with the spectrum derived from the *hybrid* data set (a fluorescence events in coincidence with at least one SD station) [3]. The agreement between the spectra derived using three different methods is good and is underpinned by the common method of energy calibration based on the FD measurements. Therefore all spectra are affected by the 21% uncertainty in the FD energy scale[1], in which the largest contribution is the absolute fluorescence yield(14%). In this work we have used the fluorescence yield reported in [11]. This common uncertainty does not affect the relative comparison of our spectra. The systematic uncertainty in the hybrid-only spectrum is dominated by uncertainties in the calculation of the exposure (16%). The systematic uncertainty in the SD spectrum has two contributions: the calculation of the exposure (3%) and the statistical uncertainty in the calibration of $S(1000)$ and N_{19} with the FD energy (<10%). We use a maximum likelihood method, together with our knowledge of the systematics, to calculate the relative normalization factors necessary to match the spectra with each other. We find that the different spectra are in excellent agreement with normalization factors smaller than 3%. We combine the three spectra weighting each bin based on its statistical uncertainty. The final combined spectrum is shown later in Fig. 3. It should be noted that the first two bins in the SD spectrum were excluded in this procedure. We expect these first two bins are biased by threshold effects of the order of 10%. The deviations of those bins from the Hybrid spectrum are in agreement within the systematic uncertainty.

The highest end of the spectrum

Since the 21% systematic uncertainty in the energy scale does not modify the shape of the spectrum, it is possible to check the continuation of the spectrum at the highest energies. It could be argued that our energy calibration has low statistics at the highest energies (see Fig. 3 in [5]). However no indication of a change in the calibration parameters with threshold energy used has been found. A dramatic change in the hadronic interactions in the energy range where no hybrid event is observed could also induce false spectral features. However, there is no theoretical basis for such a scenario, and even if it was the case it will be checked in the future with larger statistics in the hybrid data set.

To check the continuation of the spectrum at the highest energies we first fit the SD spectrum between $10^{18.6}$ eV and $10^{19.6}$ eV to a power-law function using a binned likelihood method. The spectral index obtained is $\gamma = 2.62 \pm 0.03(\text{stat}) \pm 0.02(\text{sys})$. The systematic error is given by the error on the calibration curve in [5]. The number of events expected from such a single power-law flux above $10^{19.6}$ eV and 10^{20} eV are 132±9 and 30±2.5 respectively whereas we observe only 58 events and 2 events. Also, the spectral index from $10^{19.6}$ eV up to the highest energy observed ($1.90 \pm 0.16(\text{stat}) \pm 0.20(\text{sys}) \times 10^{20}$ eV) is $\gamma = 4.14 \pm 0.42(\text{stat})$ (Fig.2). A lack of events at the highest energies is clear. We then applied

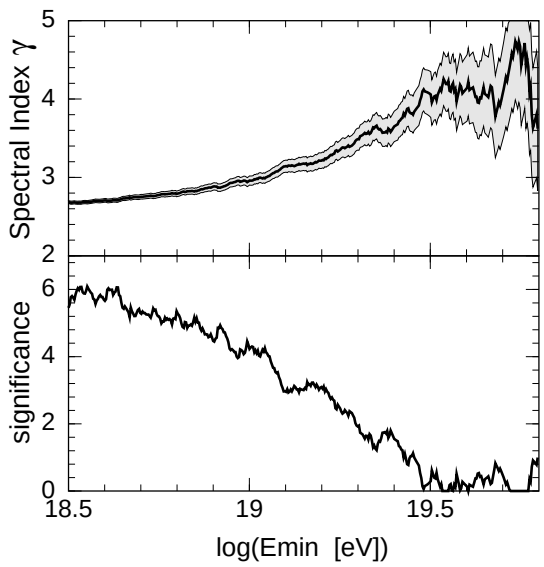

Figure 2: Upper panel: Spectral index as a function of minimum energy in the fit. Lower panel: significance (in sigma) of the deviation from power-law distribution with spectral index from upper panel based on the TP statistics.

a statistical test proposed in [13], the so called TP-test (see [14] for details). The TP statistic allows us to test for a power-law distribution on an unbinned data set without bias regarding the value of the spectral index. Details of this statistical test can be found in [14]. The upper panel in Fig.2 shows the unbinned maximum-likelihood estimation of the spectral index (γ) and its standard deviation (shaded region) as a function of minimum energy used in the fitting. A clear change of slope at the highest energy can be seen. The deviation from the power-law distribution with γ shown in this figure is estimated based on the TP statistic. The lower panel in Fig.2 shows the estimated deviation in sigma. The hypothesis of the pure power-law is then rejected with a significance better than 6 sigma and 4 sigma for minimum energies of $10^{18.6}$ eV and 10^{19} eV respectively.

Astrophysical interpretation

In the previous section, we have shown that the rejection of the hypothesis of a continuation of the spectrum in the form of a power-law is statistically significant. Moreover, a spectral break at $\sim 10^{18.5}$ eV, the so-called *ankle*, is apparent in Fig. 1. Therefore we fitted the combined Auger spectrum to the following equation:

$$\begin{aligned} J(E; E < E_{ankle}) &\propto E^{-\gamma_1} \\ J(E; E > E_{ankle}) &\propto E^{-\gamma_2} \frac{1}{1+\exp\left(\frac{\lg E - \lg E_c}{W_c}\right)} \end{aligned} \quad (1)$$

where γ_1 and γ_2 are the spectral index before and after the break respectively, E_{ankle} is the position of the break, and the second term in the second equation is a flux suppression term where E_c is the energy at which the flux is suppressed 50% compared to a pure power-law, and W_c determines the sharpness of the cut-off. Here using a binned likelihood method, the values of the parameters obtained are the following: γ_1=3.30±0.06, γ_2=2.56±0.06, $log_{10}E_{ankle}$=18.65±0.04, $log_{10}E_c$=19.74±0.06 and W_c=0.16±0.04. The χ^2/dof for this fit is 16.7/16. The black line in Fig. 3 shows the result of the fit.

Fig. 3 shows also a comparison of our data with some astrophysical models [9]. The predicted total flux has been normalized to our data at 10^{19} eV. These models show a flux suppression at the highest energies (the GZK steepening [15, 17]). The models all assume an injection spectral index, an exponential cutoff at an energy of E_{max} times the charge of the nucleus, and a mass composition at the acceleration site as well as a distribution of sources. The blue lines in the figure assume a mixed composition at the sources, i.e. with nuclear abundances similar to those of the low-energy galactic cosmic rays. A uniform distribution of sources and an injection spectral index of 2.2 (close to the shock acceleration predictions) are assumed as indicated in the figure. E_{max} is taken as 10^{20} eV (solid line) and 10^{21} eV (dashed line). Good agreement is found down to ener-

gies close to E_{ankle}, where another component (possibly a Galactic one) emerges. Another set of models which assume only proton primaries and $E_{max} = 10^{20}$ eV are shown by the red lines. One model assumes uniform source distribution with the spectral index 2.2 and the other assumes the source evolution has a redshift dependence proportional to the star formation rate (SFR) with the spectral index 2.3. It has been suggested that the spectral break at E_{ankle} can be explained as a feature of the propagation of a pure proton flux in the extragalactic media including $e^{\pm}$ pair production [12]. To reproduce our spectrum by this model, we need a much stronger source evolution. The distribution of the longitudinal profiles of the showers observed by the FD also disfavors the pure proton assumption [6].

Conclusions

Using data from the southern-hemisphere Pierre Auger Observatory, we reject the hypothesis that the cosmic ray spectrum continues in the form of a power-law above an energy of $10^{19.6}$ eV with 6 sigma significance. This result is independent of the systematic uncertainties in the energy scale. A precise measurement of the energy spectrum, together with anisotropy and mass composition studies in this energy range, will shed light on the origin of the highest energy particles observed in nature.

References

[1] B.R. Dawson [Pierre Auger Collaboration]. these proceedings, (2007) #0976.
[2] D. Newton [Pierre Auger Collaboration]. these proceedings, (2007) #0308.
[3] L. Perrone [Pierre Auger Collaboration]. these proceedings, (2007) #0316.
[4] M. Ave [Pierre Auger Collaboration]. these proceedings, (2007) #0297.
[5] M. Roth [Pierre Auger Collaboration]. these proceedings, (2007) #0313.
[6] M. Unger [Pierre Auger Collaboration]. these proceedings, (2007) #0594.

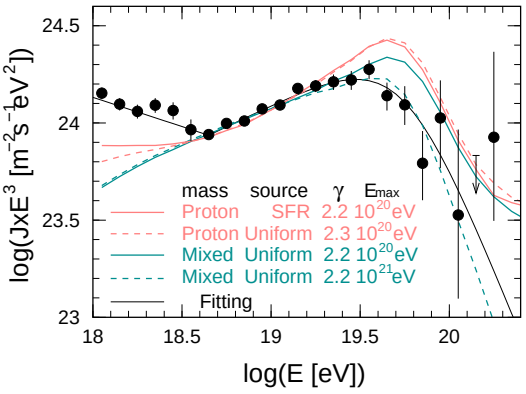

Figure 3: The combined energy spectrum multiplied by E^3, together with a fit to Eq. 1 (black line), and the predictions of two astrophysical models (blue and red lines). The input assumptions of the models (mass composition at the sources, the source distribution, spectral index and exponential cutoff energy per nucleon at the acceleration site) are indicated in the figure.

[7] P. Facal [Pierre Auger Collaboration]. these proceedings, (2007) #0319.
[8] R. Engel [Pierre Auger Collaboration]. these proceedings, (2007) #0605.
[9] A.V Olinto D. Allard, E. Parizot. Astropart. phys., (2007), **27**, 61-75, astro-ph/0512345.
[10] H. Barbosa et. al. Astropart. phys., (2004), **22**, 159.
[11] Nagano et al. Astrop. phys., (2004), **22**, 235-248.
[12] V. Berezinsky et al. Phys. rev., (2006), **d 74**, 0403005, hep-ph/0204357.
[13] V. Pisarenko *et al.* Computational seismology, (2004), **35**, 138-159.
[14] J. D. Hague *et al.* [Pierre Auger Collaboration]. these proceedings, (2007) #1217.
[15] K. Greisen. Phys. rev. lett., (1966), **16**, 748.
[16] D. Heck T. Pierog, R. Engel. Czech. j. phys., (2006), **56**, 161-172, astro-ph/060219.
[17] G.T. Zapsetin and V.A. Kuzmin. Sov. phys. jetp lett., (1966), **4**, 78.